HHS Public Access

Author manuscript

Proc SPIE Int Soc Opt Eng. Author manuscript; available in PMC 2022 April 08.

Published in final edited form as:

Proc SPIE Int Soc Opt Eng. 2021 February ; 11595: . doi:10.1117/12.2581944.

High Resolution, Full Field-of-View, Whole Body Photon-Counting Detector CT: System Assessment and Initial Experience

Kishore Rajendran[*,a], **Jeff Marsh**[a], **Martin Petersilka**[b], **André Henning**[b], **Elisabeth Shanblatt**[c], **Bernhard Schmidt**[b], **Thomas Flohr**[b], **Joel Fletcher**[a], **Cynthia McCollough**[a], **Shuai Leng**[a]

[a]Department of Radiology, Mayo Clinic, Rochester, MN, USA

[b]Siemens Healthcare GmbH, Forchheim, Germany

[c]Siemens Medical Solutions USA Inc., Malvern, PA, USA

Abstract

Computed tomography (CT) using photon-counting detectors (PCD) offers dose-efficient ultra-high-resolution imaging, high iodine contrast-to-noise ratio, multi-energy and material decomposition capabilities. We have previously demonstrated the potential benefits of PCD-CT using phantoms, cadavers, and human studies on a prototype PCD-CT system. This system, however, had several limitations in terms of scan field-of-view (FOV) and longitudinal coverage. Recently, a full FOV (50 cm) PCD-CT system with wider longitudinal coverage and higher spatial resolution (0.15 mm detector pixels) has been installed in our lab capable of human scanning at clinical dose and dose rate. In this work, we share our initial experience of the new PCD-CT system and compare its performance with a state-of-the-art 3rd generation dual-source CT scanner. Basic image quality was assessed using an ACR CT accreditation phantom, high-resolution performance using an anthropomorphic head phantom, and multi-energy and material decomposition performance using a multi-energy CT phantom containing various concentrations of iodine and hydroxyapatite. Finally, we demonstrate the feasibility of high-resolution, full FOV PCD-CT imaging for improved delineation of anatomical and pathological features in a patient with pulmonary nodules.

Keywords

Photon-counting detectors; X-ray computed tomography; ultra-high spatial resolution; multi-energy CT; image quality

1. INTRODUCTION

Photon-counting detectors, unlike conventional energy-integrating detectors (EID) used in commercial CT, use direct conversion technology for x-ray detection. This leads to uniform

* rajendran.kishore@mayo.edu; phone 1 507-284-1765.

photon weighting[1–3], and consequently improved image contrast[4]. Additionally, PCD pixels do not suffer from fill factor limitations like EIDs, thereby eliminating the need for inter-pixel reflective septa. This allows the design of smaller detector pixels for ultra-high resolution (UHR) imaging. In conventional CT, UHR capability is typically achieved using comb filters to reduce the detector pixel aperture[5], which is a dose-inefficient approach since the filter blocks x-rays that have passed through the patient. With PCDs, UHR imaging can be achieved using small detector pixels without the need for comb filters, resulting in increased dose efficiency[6–8]. In addition to the high-resolution capabilities, PCDs offer multi-energy imaging at single kV through energy thresholding and binning. Each PCD pixel can offer 2 or more energy thresholds for single-kV multi-energy imaging, which could be used to resolve and quantify material densities using material decomposition techniques[9–13].

We have previously demonstrated the aforementioned capabilities and benefits of PCD-CT in a whole-body research PCD-CT system (SOMATOM CounT, Siemens Healthcare GmbH) using phantoms, animals and patient studies[1, 14, 15]. This prototype system, however, had several limitations. The system was built on a 2nd generation dual-source CT scanner platform, with a limited scan FOV of 27.5 cm. To scan objects larger than the PCD FOV, an additional low dose data completion scan[16] using the orthogonal EID subsystem was required to avoid data truncation artifacts. The z-coverage was 16 mm which limited overall scanning speed. There were two detector pixel sizes available on the system (standard - 0.5 mm and UHR - 0.25 mm at isocenter). In this work, we present the initial results from a new investigational PCD-CT system with substantial improvements over the prior prototype.

The new single-source scanner enables full FOV (50 cm) for PCD-CT data acquisition. Since the PCD scan is performed at full 50 cm FOV, no additional data completion scan is required. The 144 × 0.4 mm collimation provides a 5.76 cm longitudinal coverage, yielding scan speed comparable to state-of-the-art commercial scanners and much faster than the previous PCD-CT prototype. It also features a smaller detector pixel (0.15 mm at isocenter) that enables even higher spatial resolution than the previous PCD-CT prototype (0.25 mm detector pixel). In this study, we performed a comprehensive assessment of this new prototype PCD-CT scanner and compared the system performance with a state-of-the-art 3rd generation dual source CT (SOMATOM Force, Siemens Healthcare GmbH).

2. METHODS

2.1 Full field-of-view photon-counting detector CT system

A whole-body PCD-CT system (SOMATOM Count Plus, Siemens Healthcare GmbH) was recently installed at our institution. The single-source scanner is equipped with a cadmium telluride PCD array, with an in-plane FOV of 50 cm. Two acquisition modes are available namely: standard mode (144 × 0.4 mm collimation, two energy thresholds) and UHR mode (120 × 0.2 mm collimation, one energy threshold). The system uses a Vectron x-ray tube (Siemens Healthcare GmbH) which can be operated with three different focal spot sizes for standard or UHR imaging. Gantry rotation times of 0.33s, 0.5s and 1.0s are available. Angular and longitudinal tube current modulation (CARE Dose4D, Siemens Healthcare GmbH) is available for patient dose optimization.

2.2 Phantom studies

Routine image quality assessment: We scanned a CT accreditation phantom (Gammex, Sun Nuclear Corporation) on the PCD-CT system using the standard mode (144 × 0.4 mm). Scan and reconstruction parameters and radiation dose (in terms of $CTDI_{vol}$) were matched as closely as possible to those of the routine abdomen protocol used in our practice. The acquisition was performed using 120 kV, 152 effective mAs, 0.5s rotation time, 0.6 pitch and 12 mGy $CTDI_{vol}$. Energy thresholds were set to 20 and 65 keV. Images were reconstructed using a Br44 kernel (weighted-filtered back projection, WFBP) at 3 mm slice thickness, 200 mm FOV, 512×512 matrix size. CT number, image noise, image uniformity, spatial resolution, and slice thickness were assessed using the phantom modules.

High resolution study: An anthropomorphic head phantom was scanned on the PCD-CT system using the UHR mode (120 × 0.2 mm). The acquisition was performed using 120 kV, 200 eff. mAs, 1s rotation time, and 0.6 pitch. The energy threshold was set at 20 keV. The same phantom was also scanned on a 3rd generation dual-source scanner (SOMATOM Force, Siemens Healthcare GmbH) using a comb-based UHR protocol (32 × 0.6 mm) for comparison, with 120 kV, 170 eff. mAs and 1s rotation time. The dose for PCD-CT and EID-CT scans were matched (approx. 30 mGy). Images were reconstructed using dedicated UHR kernels (Ur77, Ur85 and Ur89 WFBP) for both EID-CT and PCD-CT, 1 mm slice thickness, 512×512 matrix size, and 80 mm FOV focusing on the inner ear region of the head phantom. Image quality, especially sharpness and artifacts, was assessed and compared side-by-side.

Multi-energy study: A multi-energy CT phantom (Gammex, Sun Nuclear Corporation) was scanned on the PCD-CT system using the standard mode. Iodine (2, 5, 10, 15 mg/cc) and bone (200 and 400 mg/cc) inserts were placed in the phantom and scanned using a head protocol – 120 kV, 210 eff. mAs, 0.5s rotation time and 36 mGy $CTDI_{vol}$. Energy thresholds were set to 20 and 65 keV. Images were reconstructed using a quantitative Qr40 kernel (WFBP) at 3 mm slice thickness, 250 mm FOV, and 512×512 matrix size.

A material decomposition framework based on prior knowledge aware iterative denoising[13] (MD-PKAID) previously developed by our group was used to quantify the concentration of each basis material from the multi-energy phantom images. The decomposition is an iterative technique that yields noise reduction in material maps. The MD-PKAID parameters are as follows: basis decomposition of three materials (iodine, bone and water), number of iterations = 300, regularization parameter (λ) = 1000 and c = 0.6. Accuracy and precision of the material quantification was assessed by comparing with the reference concentrations.

2.3 Patient study

A patient clinically indicated for pulmonary nodules was scanned on a 3rd generation CT scanner (SOMATOM Force, 192 × 0.6 mm, 120kV, CARE Dose4D, quality reference mAs = 80, CTDIvol = 6.3 mGy) and on the PCD-CT system (SOMATOM Count Plus, 120 × 0.2 mm, 120kV, energy threshold = 20 keV, CARE Dose4D, quality reference mAs = 70, $CTDI_{vol}$ = 6 mGy). EID-CT images were reconstructed with Qr54 kernel, 1024 matrix size, 0.75 mm slice thickness using iterative reconstruction (strength 3) at 440 mm FOV;

PCD-CT images were reconstructed using Qr56 kernel, 1024×1024 matrix size, 0.6 mm slice thickness using iterative reconstruction (strength 3) at 440 mm FOV.

3. RESULTS AND DISCUSSION

PCD-CT images of the ACR phantom at threshold low (20 to 120 keV) and threshold high (65 to 120 keV) are shown in Figure 1. The spatial resolution module demonstrates that up to 8 lp/cm are resolvable using the standard abdominal routine protocol, with standard mode (144 × 0.4 mm) and medium smooth kernel (Br44). The CT number of water was well within the ±5HU limit required by the American College of Radiology. The mean and standard deviation measured in the ROI exhibit clinically acceptable image uniformity (maximum difference between a peripheral and central ROI was 2.4 HU for the low threshold image and 1.6 HU for the high threshold image). The measured slice thickness was 3.5 mm for a nominal 3 mm reconstruction.

Sample images of the anthropomorphic head phantom from the PCD-CT and commercial EID-CT (Siemens Force) are shown in Figure 2. These images were reconstructed using 3 kernels with different sharpness. PCD-CT images with smaller detector pixel size outperformed EID-CT with comb filter, showing sharper images and better delineation of fine structures. For different kernels, EID-CT images show increased image noise when sharper kernels (Ur85 and Ur89) are used, diminishing the potential benefits of utilizing these sharper kernels. As a result, Ur77 is the sharpest kernel used in our clinical practice. In comparison, PCD-CT can achieve continuous improvement of image sharpness when very sharp kernels (such as Ur85 and Ur89) are used without generating substantial noise or artifacts. This enables the utilization of sharpest kernel in clinical practice to reach the full potential of the CT scanner enabled by the hardware (e.g. small size of detector cell and focal spot). This difference between EID-CT and PCD-CT could be attributed to the intrinsic resolution of the two systems. The final image resolution is dependent on the system resolution (focal spot size and detector pixel size) combined with the kernel resolution. The PCD-CT system with 0.15 mm detector pixel aperture (isocenter) results in better intrinsic system resolution compared to EID-CT, thereby allowing the use of sharper convolution kernels for reconstructions.

The multi-energy CT phantom images are shown in Figure 3. The low and high threshold PCD-CT images (20–120 keV and 65–120 keV) processed using MD-PKAID produced iodine and bone maps. The material maps show successful delineation of the iodine and hydroxyapatite inserts. The mean and standard deviation for measured iodine and hydroxyapatite concentrations are shown in Table 1. Accurate quantification was achieved with the root-mean-squared error (RMSE) between true and measured concentrations of 0.38 mg/mL for iodine and 6.15 mg/cc for hydroxyapatite. EID-CT and PCD-CT images from the chest patient study are shown in Figure 4. The UHR PCD-CT acquisition yielded superior spatial resolution and visibly improved the conspicuity of key diagnostic details such as semi-solid and sub-solid nodules, airways and cystic airspaces. Clinically, comb-based EID UHR technique is limited to inner ear and extremities; the comb filter blocks x-rays that have already passed through the patient resulting in radiation dose inefficiency. Unlike EIDs, the UHR imaging in PCD-CT is enabled by smaller detector pixels and does

not require comb filters, inherently resulting in dose-efficient UHR imaging that can be readily extended to other body parts such as chest, shoulders and pelvis.

4. CONCLUSIONS

We have presented our initial imaging experience from a high resolution, full field-of-view whole-body PCD-CT scanner using phantom experiments, and demonstrated clinical feasibility using a chest patient exam. The PCD-CT system with 0.15 mm detector-pixel aperture at isocenter offers high in-plane spatial resolution that outperforms comb-based UHR mode of commercial scanners and provides scan FOV and longitudinal coverage suitable for clinical diagnostic imaging. The system offers multi-energy capability at standard resolution (144 × 0.4 mm collimation) suitable for material decomposition tasks. Additional patient studies are underway to systematically evaluate the clinical benefits of the high resolution, multi-energy PCD-CT in various clinical areas.

ACKNOWLEDGEMENTS

Research reported in this work was supported by the National Institutes of Health under award number R01 EB028590 and C06 RR018898. The content is solely the responsibility of the authors and does not necessarily represent the official views of the National Institute of Health. Research support for this work was provided, in part, to Mayo Clinic from Siemens Healthcare GmbH. The research CT system used in this work was provided by Siemens Healthcare GmbH; it is not commercially available. The authors thank Nikkole Weber, Holly Kasten and Yong Lee for patient recruitment and scanning.

REFERENCES

1. Leng S et al. , “Photon-counting Detector CT: System Design and Clinical Applications of an Emerging Technology,” Radiographics 39(3), 729–743 (2019). [PubMed: 31059394]
2. Schmidt TG, “Optimal “image-based” weighting for energy-resolved CT,” Med Phys 36(7), 3018–3027 (2009). [PubMed: 19673201]
3. Willemink MJ et al. , “Photon-counting CT: Technical Principles and Clinical Prospects,” Radiology 289(2), 293–312 (2018). [PubMed: 30179101]
4. Gutjahr R et al. , “Human Imaging With Photon Counting-Based Computed Tomography at Clinical Dose Levels: Contrast-to-Noise Ratio and Cadaver Studies,” Investigative radiology (2016).
5. Flohr TG et al. , “Novel ultrahigh resolution data acquisition and image reconstruction for multi-detector row CT,” Med Phys 34(5), 1712–1723 (2007). [PubMed: 17555253]
6. Klein L et al. , “Effects of Detector Sampling on Noise Reduction in Clinical Photon-Counting Whole-Body Computed Tomography,” Invest Radiol 55(2), 111–119 (2020). [PubMed: 31770298]
7. Leng S et al. , “Dose-efficient ultrahigh-resolution scan mode using a photon counting detector computed tomography system,” J Med Imaging (Bellingham) 3(4), 043504 (2016). [PubMed: 28042589]
8. Pourmorteza A et al. , “Dose Efficiency of Quarter-Millimeter Photon-Counting Computed Tomography: First-in-Human Results,” Invest Radiol 53(6), 365–372 (2018). [PubMed: 29595753]
9. Gronberg F et al. , “Feasibility of unconstrained three-material decomposition: imaging an excised human heart using a prototype silicon photon-counting CT detector,” Eur Radiol 30(11), 5904–5912 (2020). [PubMed: 32588212]
10. Muenzel D et al. , “Spectral Photon-counting CT: Initial Experience with Dual-Contrast Agent K-Edge Colonography,” Radiology 283(3), 723–728 (2017). [PubMed: 27918709]
11. Roessl E, and Proksa R, “K-edge imaging in x-ray computed tomography using multi-bin photon counting detectors,” Phys Med Biol 52(15), 4679–4696 (2007). [PubMed: 17634657]
12. Symons R et al. , “Photon-counting CT for simultaneous imaging of multiple contrast agents in the abdomen: An in vivo study,” Med Phys 44(10), 5120–5127 (2017). [PubMed: 28444761]

13. Tao S et al. , “Material decomposition with prior knowledge aware iterative denoising (MD-PKAID),” Phys Med Biol 63(19), 195003 (2018). [PubMed: 30136655]
14. Bartlett DJ et al. , “High-Resolution Chest Computed Tomography Imaging of the Lungs: Impact of 1024 Matrix Reconstruction and Photon-Counting Detector Computed Tomography,” Invest Radiol 54(3), 129–137 (2019). [PubMed: 30461437]
15. Rajendran K et al. , “Quantitative Knee Arthrography in a Large Animal Model of Osteoarthritis Using Photon-Counting Detector CT,” Invest Radiol 55(6), 349–356 (2020). [PubMed: 31985604]
16. Yu Z et al. , “How Low Can We Go in Radiation Dose for the Data-Completion Scan on a Research Whole-Body Photon-Counting Computed Tomography System,” Journal of computer assisted tomography (2016).

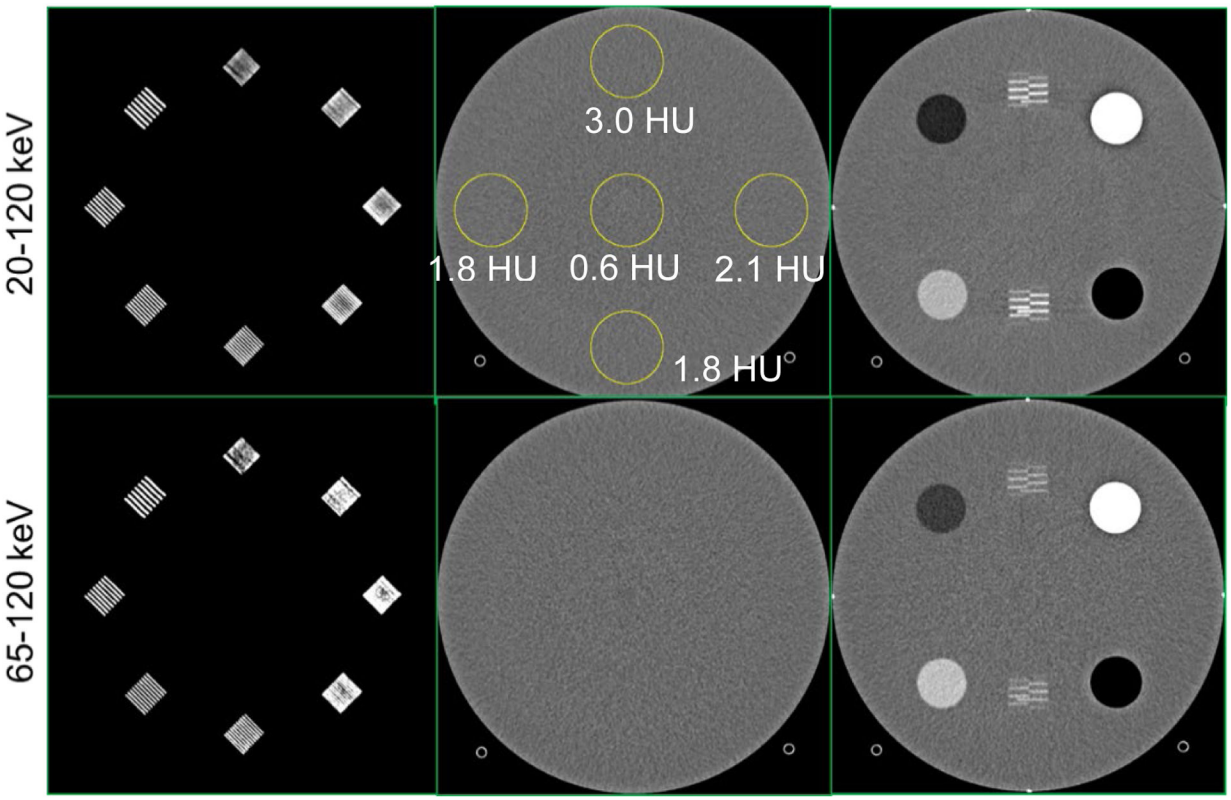

Figure 1.

PCD-CT threshold images from the ACR phantom scan. The images were acquired with the standard mode (144 × 0.4 mm) using a clinical abdomen protocol (120 kV, 12 mGy) and reconstructed using Br44 kernel at 3 mm slice thickness. Up to 8 lp/cm was resolved in both the threshold images (spatial resolution module, first column). The mean CT numbers in the circular ROIs were within ±5HU (uniformity module, middle column). The measured slice thickness was 3.5 mm for a reconstruction with 3 mm slice thickness (positioning module, third column).

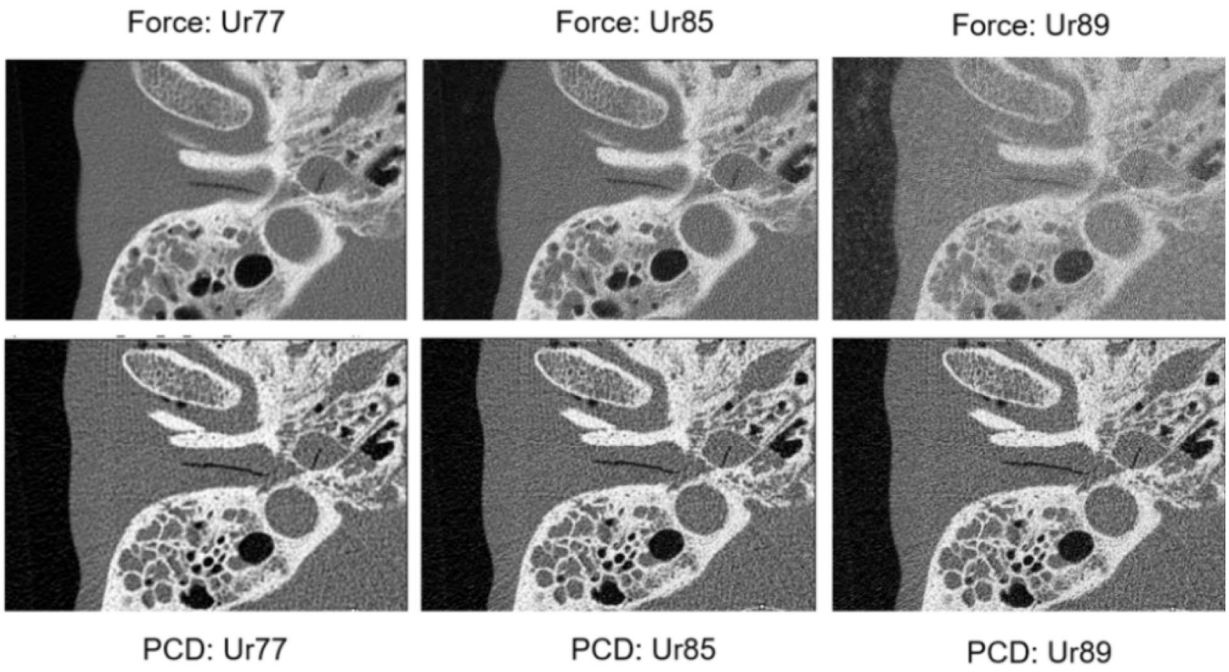

Figure 2:
EID-CT and PCD-CT images of the anthropomorphic head phantom reconstructed with 3 kernels at increased sharpness. The PCD-CT system allows the use of very sharp kernels (Ur85 and Ur89) whereas EID-CT images reconstructed with the same kernels result in substantially increased image noise.

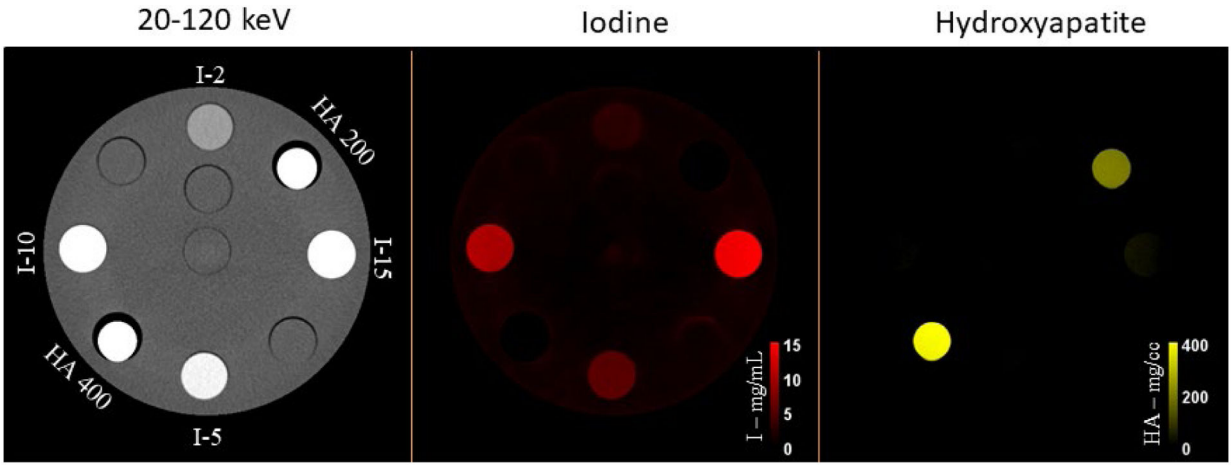

Figure 3.

PCD-CT threshold low image (20–120 keV) of the multi-energy CT phantom showing various concentrations of iodine (2, 5, 10 and 15 mg/mL) and HA (200 and 400 mg/cc). After material decomposition, iodine and HA inserts are well delineated in the iodine and bone maps, respectively, with accurate quantification of concentrations with reference to ground truth (RMSE = 0.38 mg/mL and 6.15 mg/cc for iodine and HA, respectively).

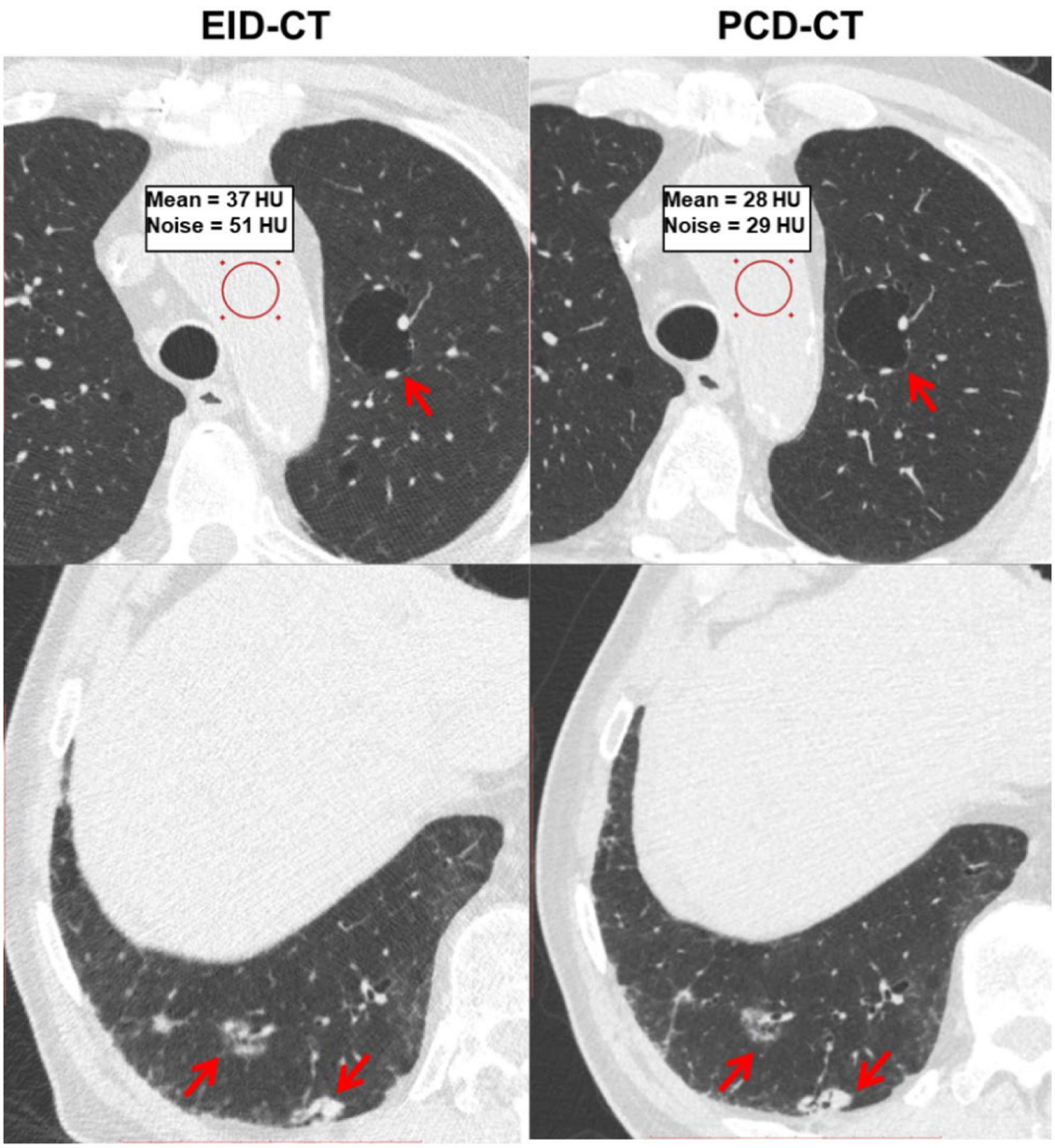

Figure 4.

Chest patient images from EID-CT and PCD-CT comparing pathological features such as cystic air spaces (red arrows, upper row) and lung nodules (red arrows, bottom row). The conspicuity of anatomic details noticeably improved in PCD-CT images. The PCD-CT image also exhibited lower image noise than EID-CT at matched acquisition dose as shown in the ROI measurements.

Table 1.

Material decomposition (MD-PKAID) accuracy and precision

Iodine conc. (mg/cc)		Hydroxyapatite conc. (mg/cc)	
True	**Measured**	**True**	**Measured**
2	2.3 ± 0.2	200	194.9 ± 5.2
5	5.1 ± 0.2	400	392.9 ± 8.3
10	9.9 ± 0.3		
15	14.3 ± 0.4		